62-1193

SYNTHESIS OF THE FORMS OF ATMOSPHERICS

By

D. S. Fligel'

UNEDITED ROUGH DRAFT TRANSLATION

SYNTHESIS OF THE FORMS OF ATMOSPHERICS

By: D. S. Fligel'

English Pages: 30

Source: Akademiya Nauk SSSR, Trudy Nauchno-Issledovatel'skogo Instituta Zemnogo Magnetizma, Ionosfery, i Rasprostraneniya Radiovoln, No. 17(27), 1960, pp. 27-49.

SC-1524
SOV/570-60-0-17-2/12

SYNTHESIS OF THE FORMS OF ATMOSPHERICS

D. S. Fligel'

Introduction

Atmospherics formed from lightning discharges are a convenient object for investigating long and super-long electromagnetic waves.

In previous works at the Institute of Terrestrial Magnetism, the Ionosphere, and Radiowave Propagation [IZMIRAN] [1, 2] it was shown that the phase velocity of the electromagnetic waves comprising atmospherics, and the effective conductivity of the lower ionosphere, can be determined by analyzing the phase (and to some extent the amplitude) characteristics of single atmospherics. A reasonably correct solution of the opposite problem was also of great interest, viz., to calculate theoretically, on the basis of a specific model of the ionosphere evolving from experimental data (see, e.g., [3]) and on the basis of experiments on the spectral properties of the source (see [2, 4, 5]), the forms of atmospherics E(t,r) expected at various distances. Comparison of the signals thus calculated with the atmospherics observed experimentally would make it possible to verify first, the correctness of the general theoretical assumptions used

for this, and second, to explain whether the effective parameters obtained theoretically for the selected ionosphere model were observed during the experiment, and if so, how frequently.

The form of the atmospherics E(t,r) has already been calculated by Budden [6] for a distance r = 1000 km from the radiator. As the radiation source he used a dipole for which the relation between the electric moment and time has the form of a step, i.e., he selected a source which did not reflect the form E(t) of the close discharges [4, 5]. It was also assumed that the ionosphere has identical conductivity over all the frequencies comprising the atmospherics. At the same time, Al'pert [3] has shown that in the range of frequencies comprising the atmospherics spectrum the effective conductivity of the ionosphere causing the propagation of these waves changes by more than 100-fold. In addition, in Budden's work [6] all calculations were made on the assumption that when r = 1000 km only one null mode participates. However, at frequencies $f \geq 15$-20 kc at this distance it is necessary to consider no less than 2-3 modes [3]. Thus although the signal obtained by Budden [6] was generally similar in form to the atmospherics observed experimentally, we could draw no further conclusions from this.*

Wait [7] has recently made similar calculations. He derives the forms of the atmospherics calculated for various distances from a source for the correct form of the source. Nonetheless, Wait [7], like Budden [6], assumes identical ionospheric conductivity for all frequencies, and the calculations are made only for one mode. Therefore the obtained signals do not show any dependence on distance and are unsuitable for any rigorous comparison with experimental data.

---

* Budden [6] did not set this as one of his tasks.

We learned of Wait's work [7] only after we had finished and formulated our investigations; these were reported on briefly [8, 9] before Wait's work was published. The present article contains more detailed results of our work.

We calculated the atmospherics for various distance from a source, taking into account the necessary number of modes and the dependence of effective conductivity of the ionosphere on frequency. We give an analysis of the calculated and observed forms of the signals from a number of their external characteristics, and a more profound analysis is given by comparison of their phase characteristics. We have confirmed the possibility [1] of determining in each specific case, by such a comparison, the effective ionospheric conductivity causing the propagation of the respective waves. The realization of this method can apparently be used for practical purposes. However, its accuracy can be evaluated only on the basis of direct measurements of the same effective ionospheric parameters.

1. Calculation Method

To calculate the form of the signal received at each distance r, i.e., to determine E vs. t and r, we must calculate the Fourier integral

$$E(t, r) = \frac{1}{2\pi} \int_{-\infty}^{\infty} g(\omega, r) Q_0(\omega, 0) e^{i\omega t} d\omega, \tag{1}$$

where

$$g(\omega, r) = B(\omega, r) e^{-i\Phi(\omega, r)} = \frac{i2\pi k^2}{h} \sum_{n=0}^{\infty} S_n^2 H_0^{(2)}(krS_n) P(C_n) \tag{2}$$

is the electric or magnetic field of a wave of frequency ω above the earth's surface [3], while

$$Q_0(\omega, 0) = A_0(\omega, 0) e^{i\varphi_0(\omega, 0)} \tag{3}$$

is the spectral radiation density of the source in its immediate vicinity.

It has been shown [4, 5] that the form of the signals excited by lightning in the immediate vicinity of the discharge is described quite well by an expression of the form

$$E_0(t, 0) = e^{-\alpha t} - e^{-\beta t},$$

while from literature data on the times of the rise and fall of a signal, Borodina [2] obtained the values

$$\alpha = (0{,}5 - 1)\cdot 10^3, \ \beta = (0{,}5 - 20)\cdot 10^4$$

and showed that a change in α and β within the indicated limits has very little effect on the amplitude characteristic of the spectrum, although its phase characteristic changes considerably. Nonetheless, we can select a "standard" source characterized by the values $\alpha = 10^3$ and $\beta = 10^5$ whose phase characteristics are

$$A_0(\omega, 0) = \frac{\beta - \alpha}{\sqrt{(\alpha^2 + \omega^2)(\beta^2 + \omega^2)}}, \qquad (4)$$

$$\varphi_0(\omega, 0) = \frac{-\omega(\beta + \alpha)}{\alpha\beta - \omega^2}.$$

As for $g(\omega, r)$, the Hankel function in expression (2) can be replaced by its asymptotic representation, when $|krS_n| > 4$-5. If, in addition, the field strength is expressed in mv/m, the current I in amperes, and h and r in kilometers, expression (2) assumes the form

$$g(\omega, r) = B(\omega, r)\, e^{-i\Phi(\omega, r)} =$$

$$= \frac{120\pi I Z_\partial}{h\sqrt{\lambda}\sqrt{r}} \left[\frac{i}{2} \sum_{n=-\infty}^{+\infty} S_n^{3/2} P(C_n)\, e^{-i\left(krS_n - \frac{\pi}{4}\right)} \right]; \qquad (5)$$

here the "complex" sine of the angle of incidence $S_n = S_{1n} + iS_{2n} = \sqrt{1 - C_n^2}$ where C_n is the root of the equation of the poles

$$2hkC_n + i \ln R = 2n\pi, \qquad (5a)$$

$$P(C_n) = \frac{1}{1 + i \frac{\partial R}{\partial C_n} \frac{1}{2hkR(C_n)}}; \qquad (5b)$$

R is the Fresnel reflection factor, a function of the complex ionospheric refraction factor and C_n; $\underline{h}$ is the height of the ionosphere; $k = \omega/c$; IZ_0 is the product of the source current, in amps, and the operating height of the radiator; and λ is the wavelength in kilometers.

For all practical purposes, when $f \geq 500$ km, expression (5) is suitable for calculating $g(\omega,r)$. In all other cases, precise values of the Hankel functions must be used [10].

Since the aspect of the function $E(t,r)$ calculated using (1) is not a function of the linear terms of the arguments of the integrands, to calculate $E(t,r)$ we must use the incomplete phase $\Phi(\omega,r)$, which has the form

$$\Phi(\omega, r) = krS_n - \arg P(C_n) - \frac{3 \arg S_n}{2} - \frac{\pi}{4},$$

and the auxiliary phase, defined by the expression

$$\psi(\omega, r) = \Phi(\omega, r) - \frac{\omega r}{c}. \tag{6}$$

Therefore, in the calculations we will deal only with $\psi(\omega,r)$. Thus, integral (1) can be represented in the form

$$E(t, r) = \frac{1}{2\pi} \int_{-\infty}^{+\infty} B(\omega, r) A_0(\omega, 0) e^{i[\omega t - \psi(\omega, r) + \varphi_0(\omega, 0)]} \cdot d\omega =$$
$$= \frac{1}{2\pi} \int_{-\infty}^{+\infty} B(\omega, r) A_0(\omega, 0) \cos(\omega t + \varphi)\, d\omega +$$
$$+ i \frac{1}{2\pi} \int_{-\infty}^{+\infty} B(\omega, r) A_0(\omega, 0) \sin(\omega t + \varphi)\, d\omega,$$

where

$$\varphi = \varphi_0(\omega, 0) - \psi(\omega, r).$$

Now we can show that the product $B(\omega,r)A_0(\omega,0)$ is an even function of the frequency, so that

$$\int_{-\infty}^{+\infty} B(\omega,r)A_0(\omega,0)\sin(\omega t + \varphi)d\omega = 0$$

and the problem reduces to one of calculating the integral

$$E(t,r) = \frac{1}{\pi}\int_0^\infty B(\omega,r)A_0(\omega,0)\cos(\omega t-\varphi)d\omega. \tag{7}$$

To calculate integral (7) it is necessary, in principle, to know the values of the integrand from zero to infinity. However, we selected integration limits from f = 5 to f = 10^5 cps. The upper limit corresponds to the frequency beginning with which the module of the integrand assumes small values and rapidly decreases. The lower limit, generally speaking, can be reduced to zero. However, the experimental data accumulated during investigations of close thunderstorms were obtained using a device which had a pass-band beginning at 100 cps; therefore we do not know how accurately (4) approximates the lightning discharge at f $\lesssim$ 100 cps. If we also take into consideration the fact that the lowest frequencies for which we investigated atmospherics are of the order of several cps, it becomes clear that it is quite sufficient to limit ourselves to the selected value of the lower limit f = 5 cps.

The wave numbers kS_n for the integration interval 5-10^5 cps were calculated as follows. For f = 500-30,000 cps we used the values of S_n obtained by Al'pert [3] for a number of discrete frequencies, while for f < 500 cps and f > 30,000 cps the values of S_n were calculated using approximate formulas derived from (5a). When 5 cps < f < 500 cps the following formulas give a good approximation:

$$C_0^2 \approx \frac{e^{i\frac{\pi}{4}}}{hk\sqrt{\beta}}; \tag{8}$$

$$S_{01} \approx 1 + \frac{1}{2\sqrt{2}hk\sqrt{\beta}}, \quad S_{02} \approx -\frac{1}{2\sqrt{2}hk\sqrt{\beta}},$$

$$C_n^2 = a^2 + 2C_0^2, \quad S_{n1} \approx \frac{1}{\sqrt{2(a^2-1)}hk\sqrt{\beta}}, \tag{9}$$

$$S_{n2} \approx -\sqrt{a^2-1}\left(1 - \frac{1}{\sqrt{2(a^2-1)}hk\sqrt{\beta}}\right).$$

where

$$n = 1, 2\ldots,\ S_n = S_{n1} + iS_{n2},\ \alpha = \frac{n\pi}{hk},$$

$$\beta = \frac{4\pi\sigma}{\omega} = \frac{4\pi Ne^2/m}{\omega\nu},$$

h is the height of the ionosphere, in km, and $k = \omega/c$. Formulas (8) were obtained under the assumption that the ionospheric conductivity σ has a rather high, but finite, value, i.e., that $4\pi\sigma/\varepsilon\omega \gg 1$, where ε is the relative permittivity. When $f \leq 5$ cps

$$S_{01} \approx \sqrt{\frac{1 + \sqrt{2}}{2\sqrt{2}hk\sqrt{\beta}}},$$
$$S_{02} \approx -\sqrt{\frac{\sqrt{2} - 1}{2\sqrt{2}hk\sqrt{\beta}}}. \qquad (10)$$

The reasonable accuracy of Formulas (8) can be seen, e.g., from a comparison, for f = 500 cps, of the values of C_0 and S_0 obtained using (8), and from the accurate formulas (see [3]). Although the criterion for the feasibility of the above-derived formulas is the inequality

$$\frac{(4\sigma)^{1/4}}{\sqrt{hk}} \gg 1,$$

and in the case given below (see Table 1) this yields $3.73 > 1$, there is nevertheless good coincidence among the corresponding data.

TABLE 1

	C_1	C_2	S_{01}	$-S_{02}$
Calculation from accurate formulas (3)	0,15	0,343	1,0476	0,0491
Calculation from approximate formulas (8)	0,141	0,341	1,0481	0,0481

As for the calculation of C_n for $f \geq 30$ kc, in this case to solve (5a) we can use (when satisfying the specific criteria [3]) the expression for the coefficient of reflection of a plane wave from a nonuniform layer recommended by Al'pert [1] for $C \ll 1$, viz.,

$$R(C) = e^{-(B_1 + iB_2)C}. \tag{11}$$

For this we calculated the dependence of the coefficient of reflection on C and the frequency for the selected ionosphere model using the Epshteyn formula for the transition zone [3]. Then the complex values of R(C) were approximated using expression (11); this made it possible to determine B_1 and B_2. Then, from the equation of the poles (5a) we found C_1 and C_2, for which we obtained the equations

$$\begin{aligned} 2hkC_{1n} - 2n\pi &= \pi - (B_2C_{1n} + B_1C_{2n}), \\ B_1C_{1n} - (B_2 + 2hk)\,C_{2n} &= 0. \end{aligned} \tag{12}$$

As a result we obtained the desired values of S_n for the entire range of frequencies f = 5-10^5 cps. Table 2 gives the values of S_o and $P(C_o)$ for the null mode; the corresponding values of S_n and $P(C_n)$ for f = 500-30,000 cps, n = 1, 2, etc., have been guven by Al'pert [3]. Figures 1-8 show graphs of S_{01}, S_{02}, $|P(C)|$, and $\arg|P(C)|$ vs. the relationship between the electron concentration and the number of collisions N/ν, obtained by Al'pert [3] for the null mode by solving the pole equations (5a) for the index of ionospheric refraction

$$n^2 \approx \left(1 - \frac{4\pi e^2 N}{m\nu^2}\right) - i\,\frac{4\pi e^2}{m\omega}\,\frac{N}{\nu},$$

applicable in the case $\nu^2 \gg \omega^2$.

These graphs can be used to determine, from the phase characteristic of the atmospherics, the values $(N/\nu)_{eff}$ vs. frequency (see below and [11]).

Using the found values of kS_n we calculated the curves of the module and the argument of integrand (1), which are the amplitude and the phase characteristic of atmospherics for various distances, viz., we constructed the curves

$$\begin{aligned} |Q_0(\omega, 0)\,g(\omega, r)| &= B(\omega, r)\,A_0(\omega, 0) = A(\omega, r), \\ \arg|Q_0(\omega, 0)\,g(\omega, r)| &= \varphi_0(\omega, 0) - \psi(\omega, r) = \varphi(\omega, r). \end{aligned}$$

TABLE 2

f'_{eps}	$\left(\frac{N}{\nu}\right)_{eff}$	S_{02}	$-S_{02}$	$\lvert P(C_0)\rvert$	arg $P(C_0)$
5	10^{-4}	1,481	0,481	0,502	0°13′
10	10^{-4}	1,340	0,340	0,503	0 14
20	10^{-4}	1,240	0,240	0,503	0 14
30	10^{-4}	1,196	0,196	0,502	0 13
40	10^{-4}	1,170	0,170	0,502	0 16
50	10^{-4}	1,152	0,152	0,501	0 16
100	10^{-4}	1,108	0,108	0,501	0 23
150	10^{-4}	1,088	0,088	0,500	0 29
200	10^{-4}	1,076	0,076	0,499	0 41
250	10^{-4}	1,068	0,068	0,498	0 52
300	10^{-4}	1,062	0,062	0,497	1 04
350	10^{-4}	1,058	0,058	0,495	1 17
400	10^{-4}	1,054	0,054	0,494	1 33
500	$7 \cdot 10^{-5}$	1,090	0,069	0,488	0 54
1 000	$3 \cdot 10^{-5}$	1,055	0,0.06	0,451	7 17
3 000	10^{-5}	0,9544	0,0499	0,9764	10 43
5 000	$4 \cdot 10^{-6}$	0,9830	0,0079	0,9275	13 57
7 000	$3 \cdot 10^{-6}$	0,9915	$3,089 \cdot 10^{-3}$	0,8830	9 46
10 000	$2 \cdot 10^{-6}$	0,9959	$1,211 \cdot 10^{-3}$	0,8713	8 49
15 000	10^{-6}	0,9978	$8,320 \cdot 10^{-4}$	0,8256	10 56
20 000	$7 \cdot 10^{-7}$	0,9985	$7 \cdot 10^{-4}$	0,7820	13 00
30 000	$5 \cdot 10^{-7}$	0,9993	$3,08 \cdot 10^{-4}$	0,7940	12 39
50 000	—	0,9998	$5,566 \cdot 10^{-5}$	0,845	9 00
100 000	—	1,000	$1,381 \cdot 10^{-5}$	0,848	8 00

* For frequencies f′ = 5-10,000 eps the effective height h_{eff} is 70 km; for f′ = 15, 20, and 30 kc, h_{eff} = 60, 50, and 50 km, respectively. In the synthesis, however, we used the value h_{eff} = 70 km for the entire frequency range.

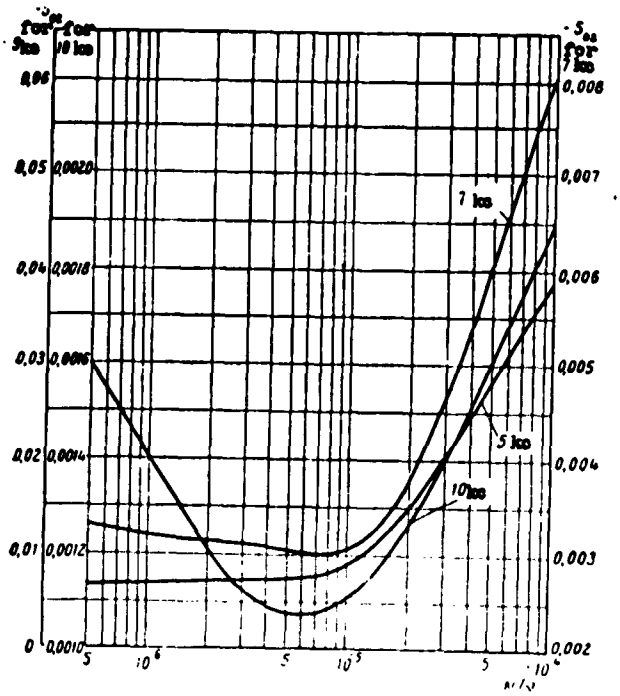

Fig. 1. Curves of S_{02} vs. N/ν for frequencies of 5, 7, and 10 kc (h_{eff} = 70 km).

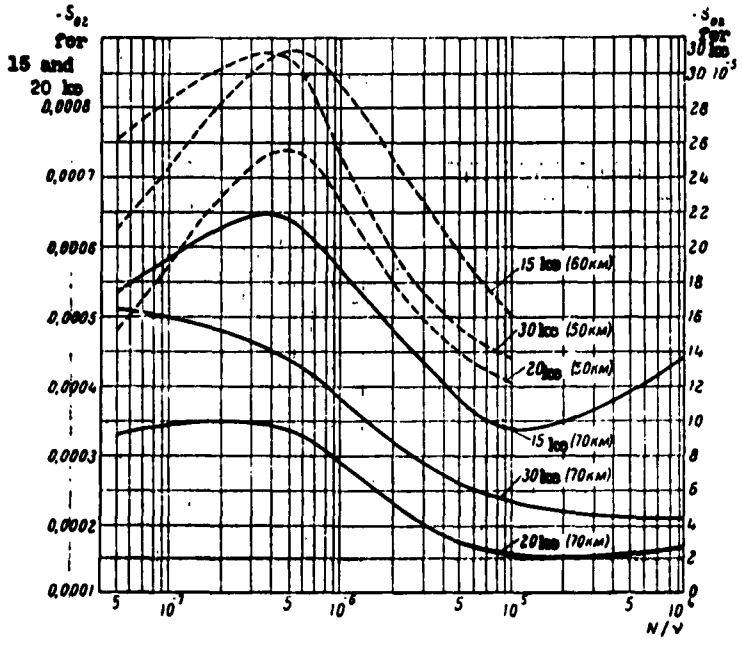

Fig. 2. Same as Fig. 1 for frequencies of 15, 20, and 30 kc (h_{eff} = 70, 60, 50 km).

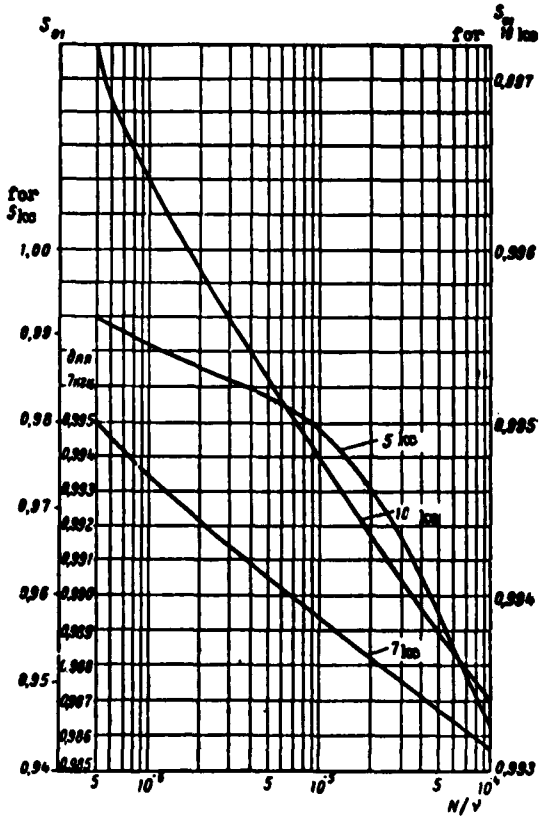

Fig. 3. Curves of S_{01} vs. N/ν for frequencies of 5, 7, and 10 kc (h_{eff} = 70 km).

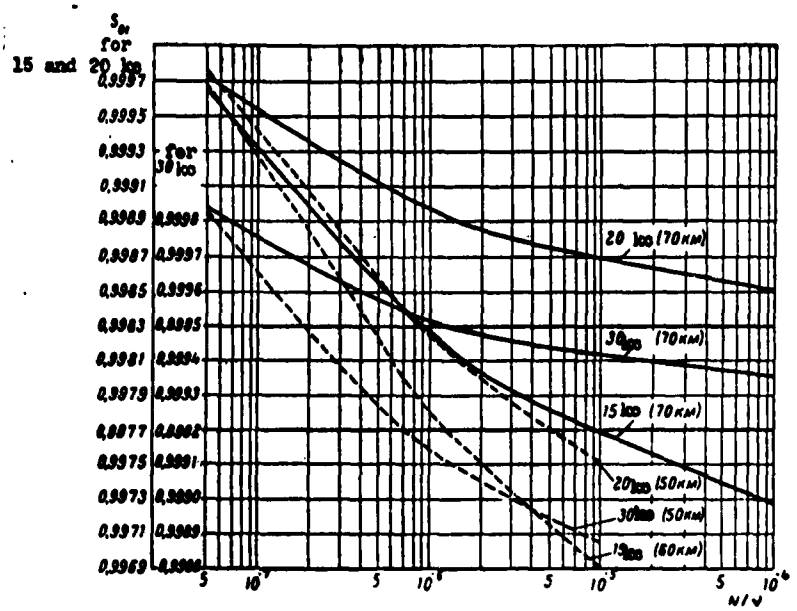

Fig. 4. Same as Fig. 3 for frequencies of 15, 20, and 30 kc (h_{eff} = 70, 60, 50 km).

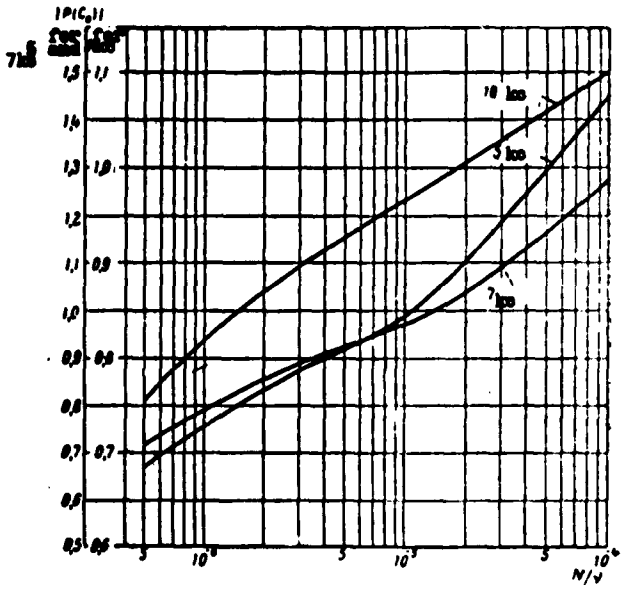

Fig. 5. Curves of $|P(C_0)|$ vs. N/ν for frequencies of 5, 7, and 10 kc (h_{eff} = = 70 km).

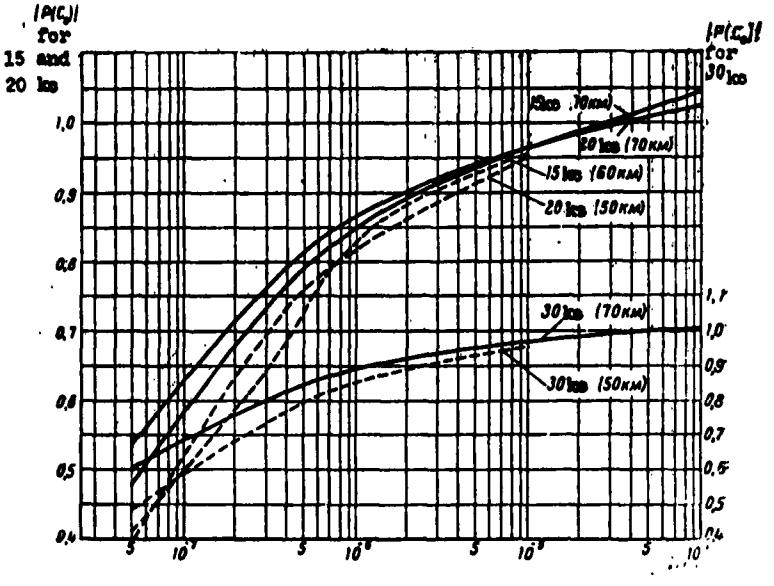

Fig. 6. Same as Fig. 5 for frequencies of 15, 20, and 30 kc (h_{eff} = 70, 60, 50 km).

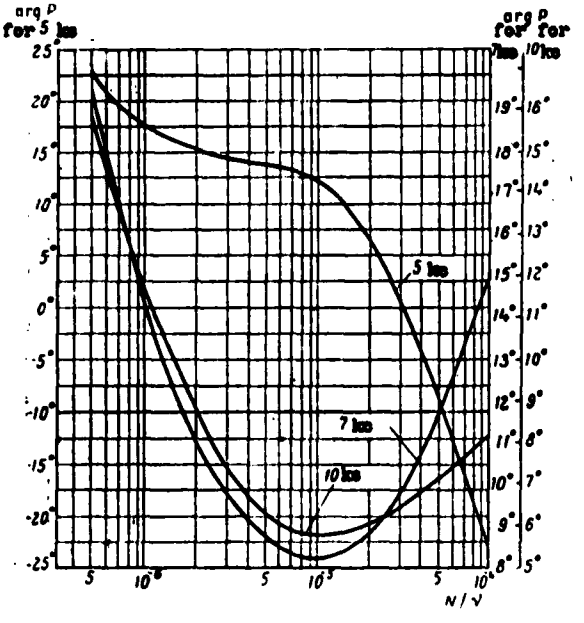

Fig. 7. Curves of arg $P(C_o)$ vs. N/ν for frequencies of 5, 7, and 10 kc (h_{eff} = 70 km).

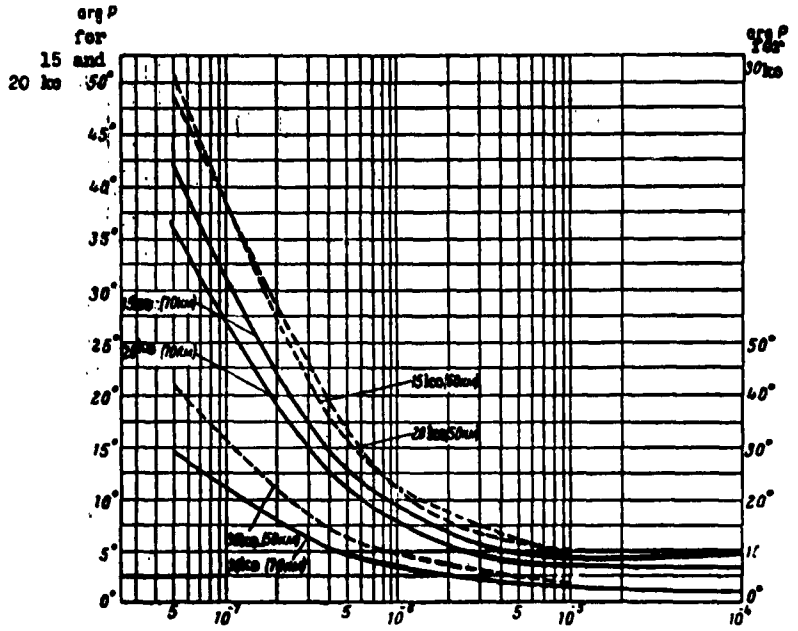

Fig. 8. Same as Fig. 7 for frequencies of 15, 20, and 30 kc (h_{eff} and h = 70 km).

From the figures it is evident that the amplitude curves have two maxima: one near 50-200 cps and a second near 5-12 kc. The first of these is displaced, with distance, toward lower frequencies; the second is displaced toward higher frequencies. The first maximum exceeds the second by a factor of 2-3.* Near 2-3 kc the amplitude curves have a minimum, the depth of which increases greatly with distance. The nature of the phase curves is also quite evident from the figures.

The number of waves n used in the calculations for various frequencies and distances was determined such that their modules were

---

* Here we should note that, as follows from [1], the ionosphere model selected for the calculations is hardly suitable for $f \leq 3$-4 kc, since at these frequencies it is apparently impossible to take into account the infiltration of waves through the ionosphere. Further, for $f \leq 200$-500 cps the source spectrum has not yet been investigated. Therefore, $|g(\omega,r)Q(\omega,0)|$ and $\arg[g(\omega,r)Q(\omega,0)]$ calculated here require further refinement for $f < 3$-4 kc. From various data we can assume that the first maxima in the frequency range 50-200 cps decrease several-fold after more precise calculations.

no less than 0.5% of the module of the most intense wave of the null mode. Although in certain cases it was equal to 6-7 (for r = 500 km), nevertheless the curves in Figs. 9-12 are reasonably smooth, since the increase in the field with decreasing frequency smooths the complex interference nature of the change in field.

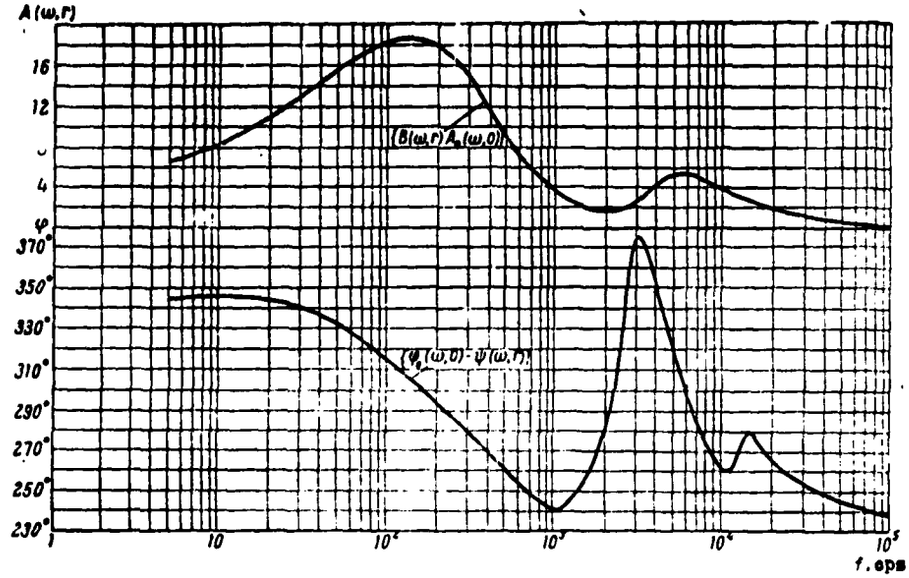

Fig. 9. The module and argument of integrand (1) vs. frequency for r = 500 km.

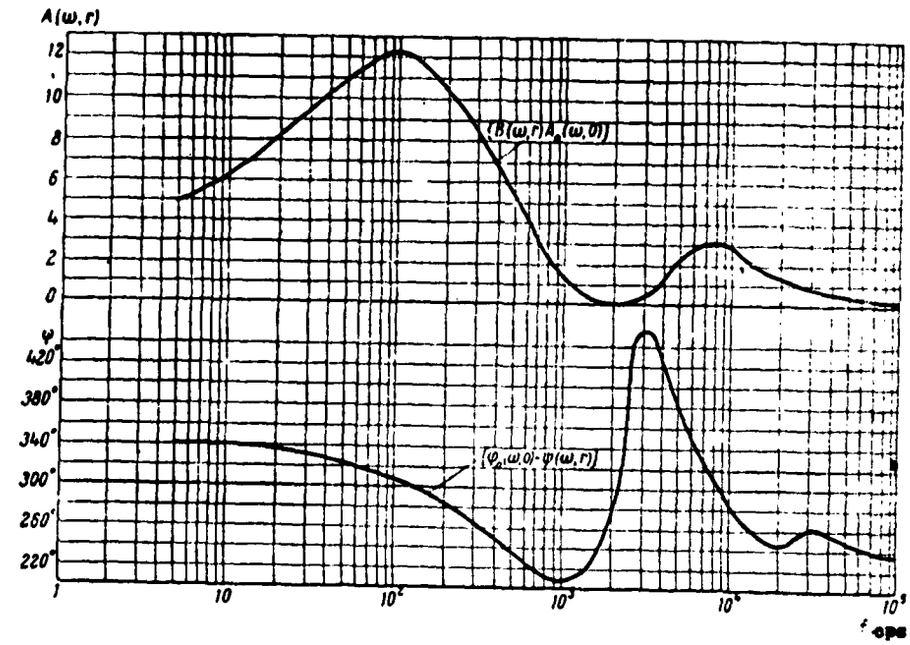

Fig. 10. Same as Fig. 9, for 4 = 1000 km.

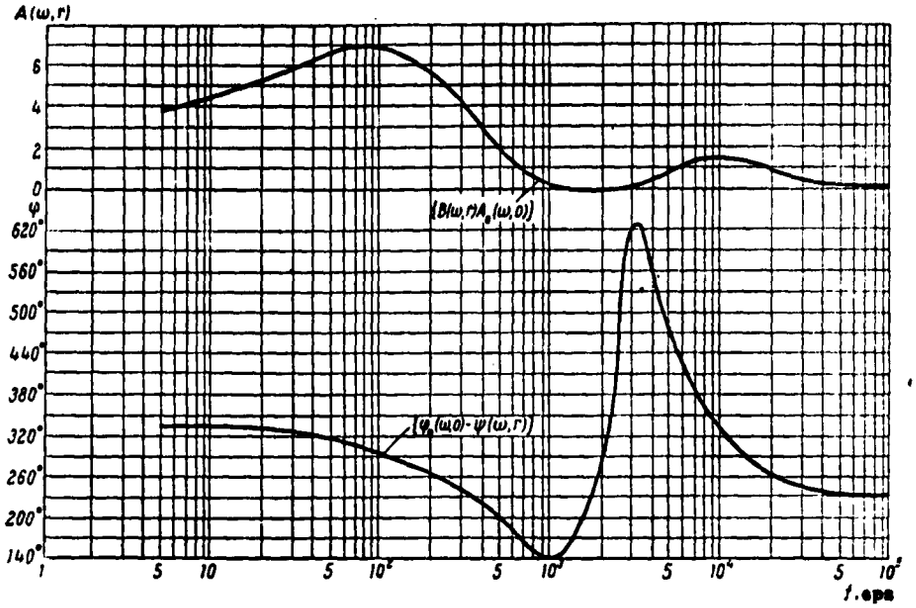

Fig. 11. Same as Fig. 9, for r = 2000 km.

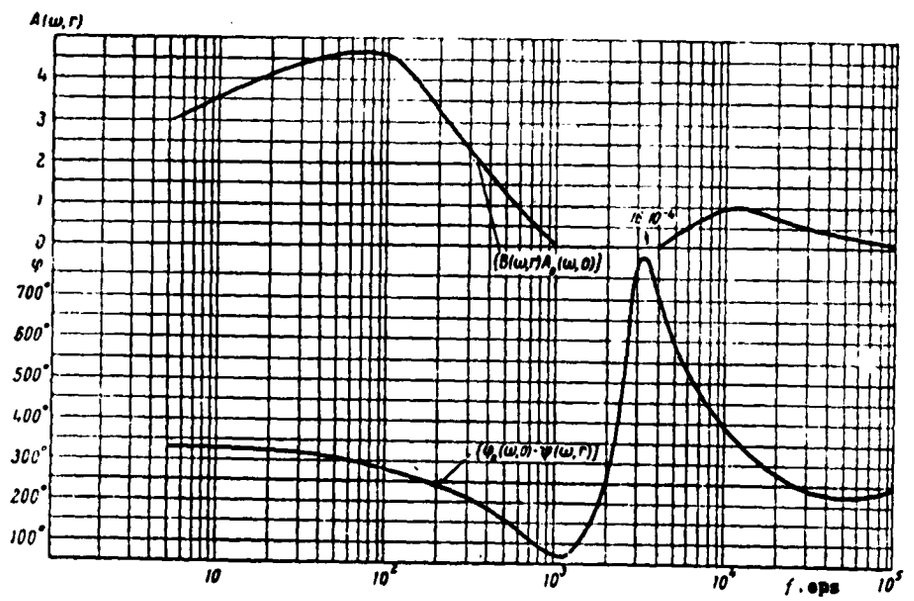

Fig. 12. Same as Fig. 9, for r = 3000 km.

To calculate integral (1), whose integrand is given using Figs. 9-12, we used numerical integration. The calculations were made in two ways.

In one of these we used the method of harmonic analysis of the

integrand; this method is as follows.

Let us rewrite (7) in the form

$$E(t,r) = \frac{1}{\pi}\int_{\omega_1}^{\omega_2} B(\omega, r) A_0(\omega, 0) \cos\varphi \cos \omega t d\omega - \tag{13}$$

$$-\frac{1}{\pi}\int_{\omega_1}^{\omega_2} B(\omega, r) A_0(\omega, 0) \sin\varphi \sin \omega t d\omega.$$

If we now determine the coefficients a_k, b_k, c_k, and d_k of the Fourier series of the expressions

$$B(\omega, r) A_0(\omega, 0) \cos\varphi = \frac{a_0}{2} + \sum_{(k)} a_k \cos\frac{2\pi k}{\omega_0}\omega + \tag{14}$$

$$+ \sum_k b_k \sin\frac{2\pi k}{\omega_0}\omega,$$

$$B(\omega, r) A_0(\omega, 0) \sin\varphi = \frac{c_0}{2} + \sum_k c_k \cos\frac{2\pi k}{\omega_0}\omega + \sum_k d_k \sin\frac{2\pi k}{\omega_0}\omega,$$

entering into integrals (13), we can obtain the following formula for calculating E(t,r):

$$E(t, r) = \frac{1}{\pi}\left\{\frac{a_0}{2t}\sin\omega_0 t + \sum_k \frac{c_k(1-\cos\omega_0 t) - a_k \sin\omega_0 t}{\left(\frac{2\pi k}{\omega_0}\right)^2 - t^2} t\right\} + \tag{15}$$

$$+\frac{1}{\pi}\left\{-\frac{c_0}{2t}(1-\cos\omega_0 t) + \sum_k \frac{2\pi k}{\omega_0}\frac{bk(1-\cos\omega t) + dk\sin\omega t}{\left(\frac{2\pi k}{\omega_0}\right)^2 - t^2}\right\},$$

which, when $t \to 2\pi k/\omega_0$, assumes the form

$$E\left(t = \frac{2\pi k}{\omega_0}, r\right) = \frac{\omega_0}{2\pi}(a_k - d_k),$$

while when t = 0

$$E(t = 0, r) = \frac{\omega_0}{2\pi} a_0. \tag{16}$$

The coefficients for expansion into Fourier series can be determined by harmonic analysis of curves (14).

The second method consisted in the approximate integration using the Simpson formula by breaking down the integration interval into the required number of parts. For this the integrand was tabulated for the interval f = 5-100,000 cps for various values of t. When using the Simpson method we can calculate E(t,r) for any values of t

(as large as we wish), which cannot be done, for all practical purposes, using the first method, since for higher harmonics the error in the harmonic analysis greatly increases.

The calculations showed that in the range f = 1000-30,000 cps, which corresponds to a signal duration of ~ 1 msec, both methods give corresponding results. However, to calculate the so-called slow "tails" of the atmospherics caused by the propagation of waves of superlow frequency f << 500-1000 cps, only the second method can be used.

2. Calculation Results; Comparison With Experimental Data

Using the method described in the previous section we calculated the signals for r = 500, 1000, 2000, and 3000 km shown in Figs. 13-16. The figures show only the so-called "high-frequency" part of the atmospherics (examined in this work) of 0.5-1 msec in duration having the form of damped oscillations with increasing period. The number of half-periods of this part of the signal changes, with increasing distance, from approximately 5 to 8; the duration of the half-period is within the limits of 30-200 msec. Behind the high-frequency part of the signal there often follows the so-called "low-frequency" part, the duration of which often reaches 10 msec and more (see interval b in Fig. 17). This part of the atmospherics (the so-called "tail") is also of an oscillatory nature but with a much larger half-period of oscillations, the number of which changes from 1 to 3 [12] and, as can easily be understood, is formed mainly by waves of frequency f << 500-1000 cps.

To compare the calculated signals with the observed atmospherics we examined 504 oscillograms recorded from September 1954 through

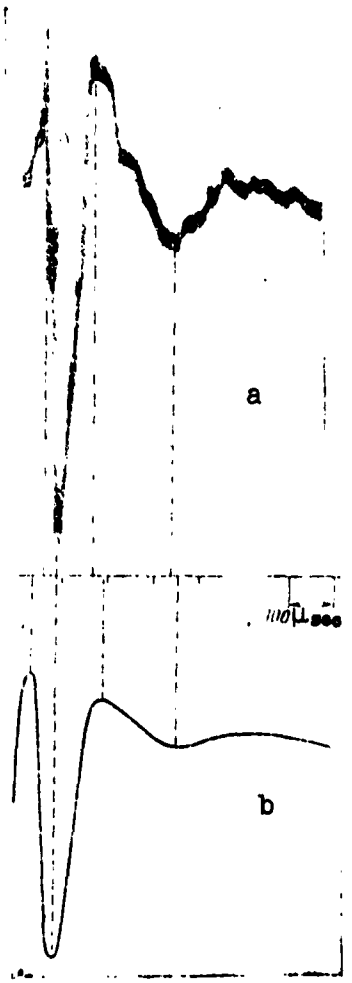

Fig. 13. Comparison of atmospherics (a) with the retically calculated signal (b) for r = 500 km.

[illegible]

Fig. 14. Same as Fig. 13, for r = 1000 km.

August 1956, i.e., almost two years. Atmospherics having irregular form were not included in the calculations; we examined only smooth atmospherics of type A [2]. Thus, of the 504 atmospherics we selected only 444 smooth atmospherics. Taking into account the accuracy in determining the distance to the source of the discharge, the examined atmospherics were grouped in the following distance groups: 400-600, 800-1200, 1800-2200, and 2700-3500 km; atmospherics between these selected intervals were not examined.

[illegible]

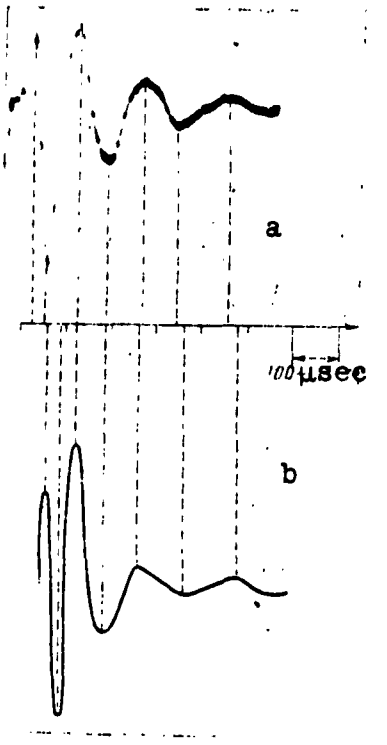

Fig. 15. Same as Fig. 13, for r = 2000 km.

Fig. 16. Same as Fig. 13, for r = 3000 km.

Figures 13-16 give, for comparison, oscillograms of atmospherics recorded at approximately these distances. From the figures it is evident that there is reasonably good external similarity between the theoretically calculated signals and the atmospherics; this is expressed in the closeness of the number of transitions $\underline{n}$ through the zero point, the duration of the high-frequency part of the atmospherics τ, and the attenuation factor α (Fig. 18).

A comparison of the signals according to these external characteristics was made on the basis of all experimental data. For this we constructed the distribution curves for $\underline{n}$ and τ (Figs. 19-22). A

corresponding analysis for the value of α was made only for the most characteristic days, i.e., those when atmospherics similar to the theoretical signal were observed, for the most part.

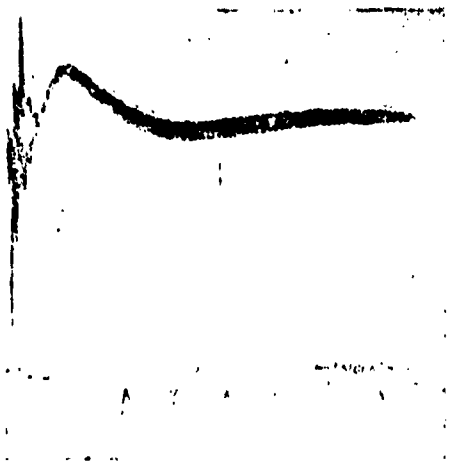

Fig. 17. Photo-oscillogram of atmospherics with the low-frequency part.

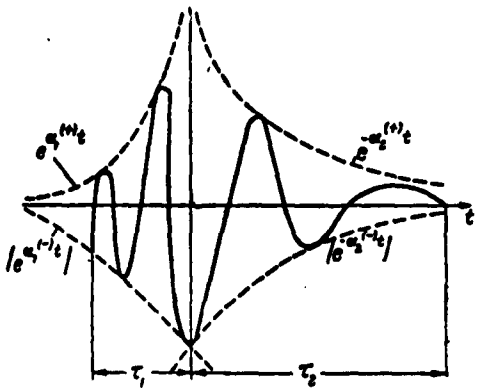

Fig. 18. Form of the atmospherics usually observed at r > 2000-3000 km.

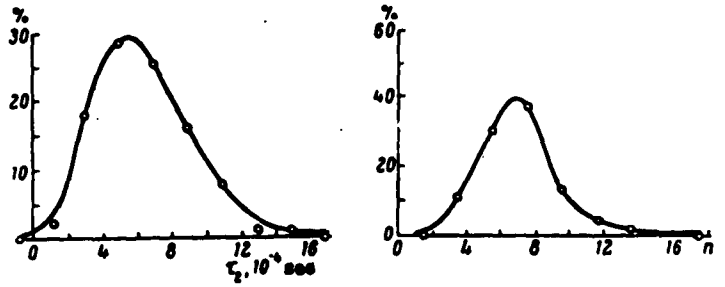

Fig. 19. Distribution curves of the number of transitions n through zero and the duration τ of the atmospherics for r = 500 km.

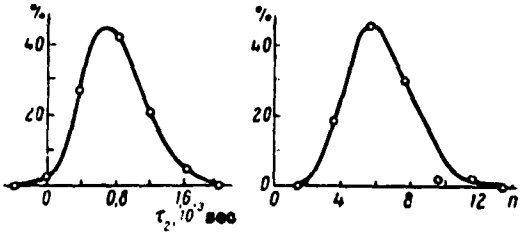

Fig. 20. Same as Fig. 19, for r = 1000 km.

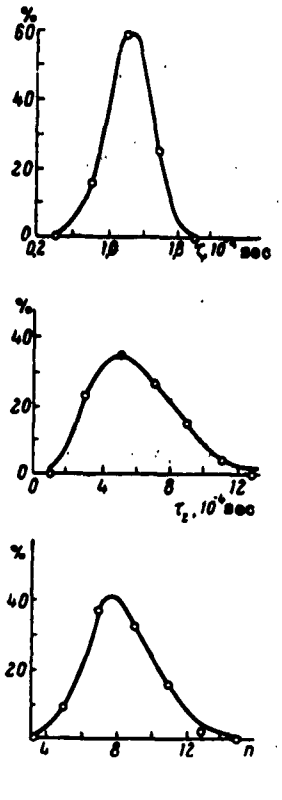

Fig. 21. Same as Fig. 19, for r = 2000 km.

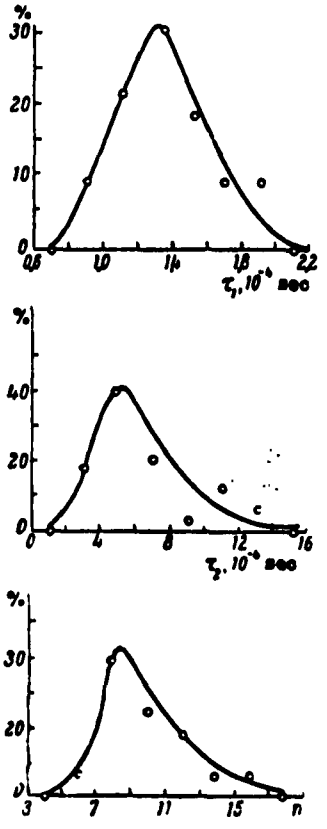

Fig. 22. Same as Fig. 19, for r = 3000 km.

The distribution of the examined atmospherics by distances, and also their number in per cents, which was similar to the theoretical according to the indicated characteristics is given in Table 3.

TABLE 3

Distance intervals, km	Total number of examined atmospherics	Number of smooth atmospherics	Number of irregular atmospherics	Number of similar ones from the number of theoretical ones, %
400—600	88	51	37	74
800—1200	167	146	21	57
1800—2200	201	200	1	48
2700—3500	48	47	1	13[1]
TOTAL:	504	444	60	

* The decrease in the number of similar atmospherics at r ≈ 2000-3000 km is explained, in particular, by the fact that here we considered atmospherics of the type shown in Fig. 18 to be dissimilar to the theoretical signals, although the corresponding values of $\underline{n}$ and τ were close (see below, Table 8).

The theoretically calculated signals (Figs. 13-16) have the values of n, α, and τ (Fig. 18) given in Table 4. From Table 4 we see that n and τ, in general, are little sensitive to a change in r.

TABLE 4

r, km	n	10^{-4} sec	10^{-4} sec	10^{3} sec^{-1}	10^{3} sec^{-1}	10^{3} sec^{-1}	10^{3} sec^{-1}
500	5	—	7	—	—	4,6	10,8
1000	7	—	6—7	—	—	6,8	8,0
2000	7	—	~7	—	—	7,0	6,5
3000	8	1	4—5	7,6	—	9,1	13,2

A comparison of the values of n and τ obtained from the maxima of the distribution curves in Figs. 19-22 with the data in Table 4 gives generally satisfactory agreement. However, beginning at distances r ~ 2000-3000 km we often note atmospherics with branches which rise and fall with time (Fig. 18), while theoretically such a form is obtained only for r ~ 3000 km, and rarely, at that. However, n and τ are close to their theoretical values.

Naturally, a more profound analysis of the similarity of the calculated and observed signals should be based on an examination of their phase and amplitude characteristics. At the same time, since an analysis of atmospherics makes it possible to determine only the behavior of the relative amplitude $\frac{B(\omega, r) A_n(\omega, 0)}{B(\omega_n, r) A_0(\omega_n, 0)}$, which changes little with distance, it is possible to obtain new data only from curves of the additional phase $\psi(\omega,r)$, which changes noticeably with distance. Since from the experiments it is impossible to determine the absolute phase values, the experimental phase curves must be fitted to the theoretical curves in the region of maximum frequencies of the examined range, where $\psi(\omega,r)$ changes little with frequency [1].

As illustration, Fig. 23 compares the behavior of the phase characteristics and Fig. 24 the behavior of the amplitude characteristics of two externally similar atmospherics at distances of approximately 1000 and 3000 km. From Fig. 23 it is evident that the phase curves of the experimental atmospherics, fitted to the theoretical curves at a frequency of 10-15 kc, are generally close to the theoretical curves right up to 3 kc. We must mention that in the majority of cases, at frequency $f < 3$ kc there is divergence of the phase and amplitude curves. All this attests to the fact that the effective ionospheric parameters selected at these frequencies evidently do not correspond to the parameters of the real ionosphere.

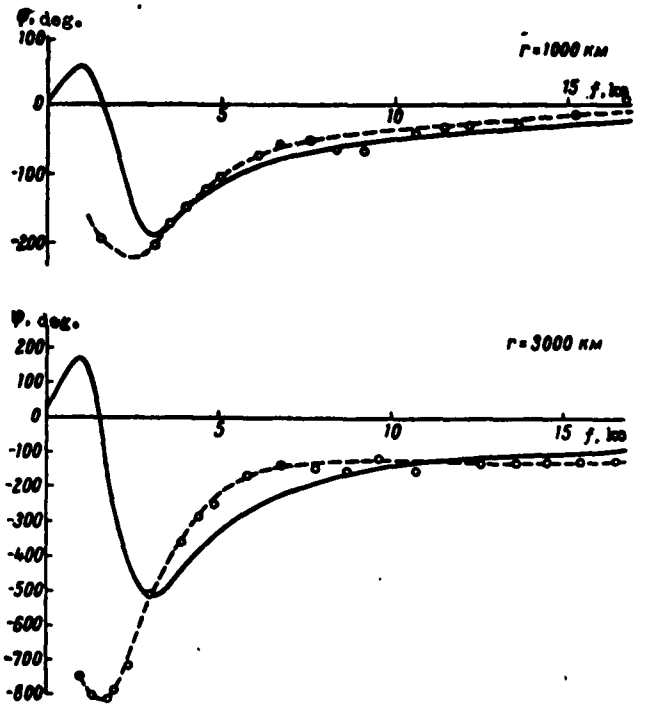

Fig. 23. Comparison of the theoretical (solid lines) and experimental (dashed lines) amplitude characteristics.

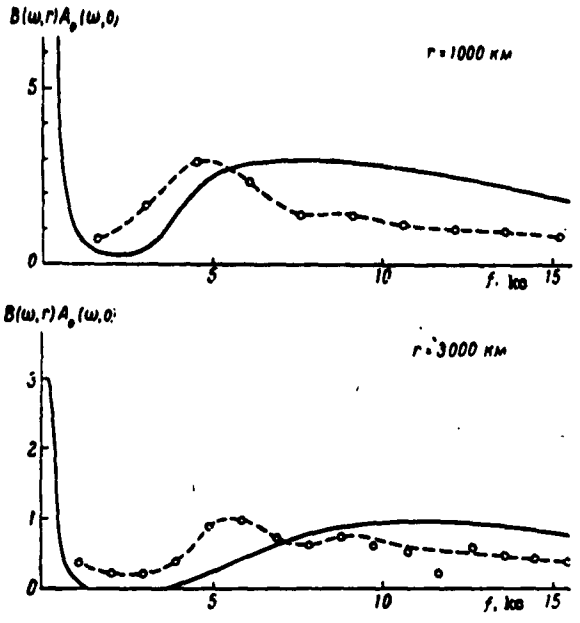

Fig. 24. Comparison of the theoretical (solid lines) and experimental (dashed lines) amplitude characteristics.

A comparison of the phase characteristics of the theoretical and experimental atmospherics is of great interest in that, as Al'pert has shown [1], it makes it possible to determine the effective parameters of the ionosphere and the rate of propagation of low-frequency waves. Since $\psi(\omega,r)$ is a function of the ionospheric conductivity, proportional to N/ν, where N is the electron concentration and ν is the number of collisions, with certain assumptions we can, from the curves $\psi(\omega,r)$, determine the values of S_{01} (Figs. 3-4) determine N/ν from data on the analysis of one or a group of atmospherics recorded under any specific conditions. With a high-speed harmonic analyzer we can obtain these data quite rapidly, i.e., use the corresponding method for practical purposes. This question has been examined in more detail by Al'pert [1]; here, however, it is interesting to make a more detailed analysis of the individual atmospherics received on various days.

We noted cases when throughout the day, practically from the same direction and distance, we received atmospherics of identical form, often similar to the theoretical signal. This made possible the conclusion that throughout the day the effective parameters of the ionosphere along a given atmospherics propagation path were reasonably constant and close to those obtained in the calculations.

For example, on July 18, 1955, we recorded 10 atmospherics, from distances of 400-600 km, from 0950 hours to 1750 hours. Two of these were of irregular form and were not examined; the remaining eight were all of identical form. It is characteristic that all atmospherics except the last came from the same direction and, consequently, had the same thunderstorm center as the source. In Table 5 we give the parameters of the atmospherics recorded during days when all smooth atmospherics were generally of approximately the same form as the theoretical signals.

TABLE 5

Date	Measurement time hr-min	Direction	Distance, km	n	τ_1, 10^{-4} sec	$e^{(+)}_{3kV}$, 10^6 sec^{-1}	$e^{(-)}_{3kV}$, 10^6 sec^{-1}
			$r \sim 500$ km				
18.VI.1955	9 49	SE	500	7	9	4,3	3,2
	12 46	S	600	7	7	5,6	5,0
	12 50	S	600	7	7	7,3	4,8
	12 51	S	500	6	7	5,7	9,7
	12 54	SSE	500	7	7	4,6	5,6
	17 46	S	600	6	6	6,3	3,6
	17 46	S	500	5	5	8,4	7,2
	17 53	E	600	5	5	8,8	6,4
10.VIII.1956	12 49	S	500	5	15	1,3	1,5
	16 45	NW	400	8	12,5	6,1	4,2
	16 49	NNW	600	8	10	4,5	5,2
30.VIII.1956	9 51	S	450	6	9,5	3,6	4,1
	9 54	S	450	7	10,5	5,0	7,9
			$r \sim 1000$ km				
24.VI.1955	17 52	SSE	1050	6	4,4	5,0	8,5
	17 56	SWbW	975	9	7	6,5	5,4
22.VI.1955	12 53	SSW	1100	6	5	8,6	5,6
	17 45	SSW	900	6	4,5	6,0	11,8
	17 51	S	900	6	4,5	5,8	5,2
	17 54	S	975	5	4	13,7	5,6
8.VI.1956	9 46	SWbW	1100	7	8,5	—	—
	9 50	SWbW	1100	9	11	—	—
	12 45	S	750	8	12,5	3,6	4,4
26.VI.1956	9 46	NE	750	7	10	—	—
	9 47	NE	850	6	5,5	4,9	7,2
	9 48	NE	750	6	6,5	6,4	7,5
	9 50	S	1100	5	3,9	6,0	2,9
	9 52	S	1000	7	7,5	7,2	7,9
4.VII.1956	12 49	W	1100	6	5,5	4,6	6,3
	16 48	W	1100	7	8	3,6	5,5
	16 48	SSW	850	6	7	4,0	2,8
	16 53	W	1100	8	11,5	2,4	4,5
	16 54	W	1050	8	10,5	5,2	4,7

TABLE 5 (continued)

Date	Measurement time hr:min	Direction	Distance, km	n	τ_s, 10^{-4} sec	$\alpha_{1av}^{(+)}$, 10^3 sec^{-1}	$\alpha_{1av}^{(-)}$, 10^3 sec^{-1}
			$r \sim 2000$ km				
27.IX.1954	9 50	SSE	1800	4	2,2	1,3	—
	9 54	SSE	2000	5	3	10,6	8,3
16.II.1954	12 53	SSW	2200	6	3,5	6,3	3,8
	12 55	SSW	1800	7	5	5,6	5,1
	17 53	SW	1800	6	4,5	5,4	7,0
12.IV.1955	9 47	SW	2200	8	6	4,1	4,8
	5 50	SSW	2000	8	9	3,2	3,0
9.V.1955	12 49	E	1950	6	3,5	5,8	7,1
	17 45	SSW	1870	6	4	7,7	10,8
22.X.1955	9 46	S	2000	7	5,5	6,1	7,7
	9 49	S	2100	5	3,5	16,7	9,2
	12 46	S	2100	7	—	—	—
	16 48	S	1900	6	4	6,0	5,1
23.III.1956	9 49	SSE	1800	7	3,7	3,4	10,0
	9 49	SSE	1875	5	2,5	20,7	9,4
	9 55	S	2025	8	6	6,5	8,4
	12 52	SSE	1950	6	3,3	6,8	3,3
			$r \sim 3000$ km				
18.IX.1954	12 50	E	3500	8	2,0	8,3	6,2
	12 57	NEbE	3300	8	4,3	5,5	11,9

Comparison of the data in Tables 5 and 4 shows quite good agreement between n, τ, and α_{av}.

When identical atmospherics, similar to the theoretical signal, were recorded at different times and from different distances and directions, the effective ionospheric parameters were evidently identical for a long period of time, not only along one path but in a rather broad region. For example, such was the case on June 25, 1956, at distances of 500 and 1000 km. On this day, no other atmospherics were observed (irregular form, nonsimilar) (Table 6).

TABLE 6

Date	Measurement time hr:min	Direction	Distance, km	n	τ_s, 10^{-4} sec	$\alpha_{1av}^{(+)}$, 10^3 sec^{-1}	$\alpha_{1av}^{(-)}$, 10^3 sec^{-1}
25.VI.1956	12 53	E	500	6	7	5,2	11,3
	16 51	SW	1000	7	8	8,2	3,11
	16 52	E	375	5	5	5,8	8,4
	16 54	SE	400	5	5	8,9	8,4
	16 56	S	850	6	6	6,3	4,7

Another such case is illustrated in Table 7. On this day one atmospheric of irregular form was also recorded.

TABLE 7

Date	Measurement time hr-min	Direction	Distance, km	n	τ_n, 10^{-4} sec	$\varepsilon^{(+)}_{\tau n}$, 10^{4} sec^{-1}	$\varepsilon^{(-)}_{\tau n}$, 10^{4} sec^{-1}
22.VI.1955	12 47	SW	1870	8	5,0	4,7	5,5
	12 53	SSW	1100	6	4,0	3,3	5,6
	17 45	SSW	900	6	4,5	6,0	11,8
	17 49	SW	1870	7	5	5,7	4,8
	17 51	S	900	6	4,5	5,8	5,2
	17 52	SW	1800	6	5	5,0	7,3
	17 54	S	975	5	4	3,7	5,6

On certain days all the recorded atmospherics, or part of them, differ externally from the calculated ones, and dissimilar atmospherics were often received from the same direction and distance, and at practically the same time. For example, on June 30, 1956, six atmospherics from a distance of approximately 1000 km were recorded. Five of these were similar to the theoretical signal and one differed from it, although they were all recorded at approximately the same time and from the same source. Another such case occurred on July 21, 1956. At present the reasons for such cases are not clear.

Table 8 gives the distribution, by days, of similar and dissimilar atmospherics. The second column gives the total number of days when atmospherics were observed from the given distance. The third column shows the number of days when only smooth atmospherics were observed (since there were days when only irregular atmospherics were observed, and these were not included in the examination). The fourth, fifth, and sixth columns give the number of days, in per cents, when we observed only similar atmospherics,* similar and dissimilar atmospherics,

* The number of similar atmospherics in Table 8 also include atmospherics of the type shown in Fig. 18, if their n and τ values are close to the values of n and τ for the theoretically calculated atmospherics.

i.e., mixed, and only dissimilar atmospherics. From Table 8 it is evident that the number of days when similar atmospherics were observed decreases with increasing distance. As we have already mentioned, the form of the atmospherics noted at distances of 2000-3000 km are obtained theoretically only for a distance of 3000 km. This can possibly be explained by the fact that in the calculations not all the features of propagation which begin to appear at great distances were taken into consideration.

TABLE 8

Distance intervals km	Total number of days when atmospherics were observed	Number of days when smooth atmospherics were observed	Number of days when only similar atmospherics were observed, %	Number of days when mixed atmospherics were observed, %	Number of days when only dissimilar atmospherics were observed, %	Number of atmospherics with two similar characteristics (n and τ), %
400—600	38	26	61,5	11,5	27	80
800—1200	63	57	45	23	32	61
1800—2200	86	86	31	31	37	60
2700—3500	31	30	7	10	83	57

Conclusion

The results of our work show that the signals calculated theoretically are in good agreement according to all external characteristics. In 40-60% of the cases, the similarity was not only qualitative but also quantitative, which indicates that in these cases the effective ionospheric parameters selected for the calculations were apparently realized. This, in turn, confirms the earlier assumption [1] that as a result of the analysis of the phase characteristics of atmospherics we can determine the effective conductivity of the ionosphere during the day for specific conditions.* There is a certain

* The present work is limited to an examination of atmospherics observed during the day, since after sunset the field is formed, in the majority of cases, by several modes, and it becomes difficult to compare theoretical data with atmospherics analysis results.

discrepancy between the form of the atmospherics and the theoretically calculated signals with increasing distance, which warrants further analysis.

In conclusion I should like to express my thanks to Ya. L. Al'pert for suggesting this question, for his leadership, and for his constant help with my work, to S. V. Borodina for her advice during my work, and to V. I. Krayushkina for her help with the calculations and setting up the tables and graphs.

REFERENCES

1. Ya. L. Al'pert. Radiotekhnika i Elektronika, 1, No. 3, 1956; S. V. Borodina, Zhurnal Eksperimental'noy i Teoreticheskoy Fiziki, 33, No. 5, 1957: Radiotekhnika i Elektronika, 4, 195, 1959.

2. S. V. Borodina. Trudy Nauchno-Issledovatel'skiy Institut Zemnogo Magnetizma, Ionosfery, i Rasprostraneniya Radiovoln, No. 13, 1956.

3. Ya. L. Al'pert. The Propagation of Low-Frequency Electromagnetic Waves Above the Earth's Surface. Moscow, Izdatel'stvo Akademii Nauk SSSR, 1955.

4. C. Bruce, and R. Golde. J.I.E.E., 88, 487, 1941.

5. J. Barlow, G. Frey, and J. Newman. J. Franklin Inst., 258, 187, 1954.

6. K. Budden. Phil. Mag., 42, 1-19, 1951.

7. J. Wait. Natl. Bur. Stan. Rept. 5513, September 3, 1957.

8. Ya. L. Al'pert, and D. S. Fligel'. Radiotekhnika i Elektronika, 4, 202, 1959.

9. Ya. L. Al'pert. Uspekhi Fizicheskikh Nauk, 60, 369, 1956.

10. Table of the Bessel Functions $J_0(z)$ and $J_1(z)$ for Complex Arguments. Columbia University Press, 1943; Table of the Bessel Functions Y(z) and Y(z)* for Complex arguments. Columbia University Press, 1950.

---

* As in original [Translator's note].

11. L. M. Brekhovskikh. Doctoral Dissertation. Fizicheskiy Institut Akademii Nauk SSSR, 1946; Izvestiya Akademii Nauk SSSR, Seriya Fizicheskaya, 8, 505; 13, 515, 594, 1949.

12. L. Lieberman. J. Appl. Phys., 27, 1473, 1477, 1956.

DISTRIBUTION LIST

DEPARTMENT OF DEFENSE	Nr. Copies
HEADQUARTERS USAF	
AFCIN-3D2	1
ARL (ARB)	1
OTHER AGENCIES	
CIA	1
NSA	6
ATD	2
OTS	2
AEC	2
PWS	1
NASA	1
RAND	1

MAJOR AIR COMMANDS	Nr. Copies
AFSC	
SCFTR	1
ASTIA	25
TD-B1a	5
TD-B1b	3
ADEC (AEY)	1
SSD (SSF)	2
APGC (PGF)	1
ESD (ESY)	1
RADC (RAY)	1
AFSWC (SWF)	1
AFMTC (MTW)	1